Finite-difference modeling of 3D seismic wave propagation in high-contrast media

Leiph A. Preston, David F. Aldridge, and Neill P. Symons, Sandia National Laboratories*

Summary

Stable and accurate numerical modeling of seismic wave propagation in the vicinity of high-contrast interfaces is achieved with straightforward modifications to the conventional, rectangular-staggered-grid, finite-difference (FD) method. Improvements in material parameter averaging and spatial differencing of wavefield variables yield high-quality synthetic seismic data.

Introduction

Interfaces between air and rock present perhaps the strongest contrast in medium properties for propagating seismic waves. Air-rock interfaces occur at the earth's surface, where the vast majority of seismic data are recorded, and in association with underground voids, caves, caverns, mines, tunnels, or other subterranean man-made facilities. Typically, the particular medium parameter with greatest contrast is mass density, ranging from ~1 kg/m^3 for air to ~2800 kg/m^3 in hard rock environments.

Seismic wave propagation modelers have long noted that time-domain finite-difference algorithms experience numerical instability problems with media containing large mass density variations. It is emphasized that these instabilities (i.e., unbounded numerical growth in wavefield variables with increasing time) are *not* generated by any violation of the CFL condition required for stable FD calculations. In all cases, the FD timestep is chosen to be sufficiently small. Rather, instability appears to be induced by an abrupt change in mass density at adjacent spatial gridpoints exceeding a critical threshold value. Recent investigations by Haney (2007), treating wave propagation in acoustic media, have quantified the mathematical conditions under which such instabilities arise. These results now need to be extended to elastic media and higher-order FD operators.

Several *ad hoc* approaches are currently utilized by FD modelers to obtain numerical stability at an air-rock interface. A popular technique involves smoothing wavespeed and/or mass density across the boundary (Frankel and Leith, 1992; Schultz, 1997; Bartel et al., 2000). However, this may entail an unacceptable change to the model, and does not necessarily lead to accurate seismic responses. The recently-developed *rotated staggered grid* method (Saenger et al. 2004) employs modified spatial FD operators that apparently enhance stability, albeit at a cost of reduced phase and group speed performance. In the present study, we introduce simple modifications into the *standard staggered grid* time-domain FD method, with the goal of maintaining stability and increasing accuracy. In particular, we adopt the material parameter averaging approach advocated by Moczo et al. (2002), and simultaneously reduce the order of spatial differencing in the immediate vicinity of high-contrast interfaces. The methodology appears to yield high-quality synthetic seismic data, while preserving the many favorable aspects of the standard staggered grid FD algorithm.

Previous studies of seismic wave propagation modeling in the presence of material discontinuities (e.g., Muir, et al., 1992; Cunha, 1993; Zahradnik, et al., 1993) attest to the continuing relevance and importance of this issue.

Seismic Data Calculation

Synthetic seismic data for an isotropic elastic medium are calculated via an explicit, time-domain, FD method. A set of nine, coupled, first-order, inhomogeneous, linear partial differential equations are solved for the particle velocity vector components $v_i(\mathbf{x},t)$ and the stress tensor components $\sigma_{ij}(\mathbf{x},t)$. In rectangular coordinates x_i (i=1,2,3), these equations, known as the *velocity-stress system*, are

$$\frac{\partial v_i}{\partial t} - \frac{1}{\rho}\frac{\partial \sigma_{ij}}{\partial x_j} = \frac{1}{\rho}\left(f_i + \frac{\partial m_{ij}^a}{\partial x_j} \right), \tag{1a}$$

$$\frac{\partial \sigma_{ij}}{\partial t} - \lambda \frac{\partial v_k}{\partial x_k}\delta_{ij} - \mu\left(\frac{\partial v_i}{\partial x_j} + \frac{\partial v_j}{\partial x_i} \right) = \frac{\partial m_{ij}^s}{\partial t}. \tag{1b}$$

δ_{ij} is the Kronecker delta symbol, and summation over repeated subscripts is implied. The elastic medium is characterized by mass density $\rho(\mathbf{x})$ and Lamé parameters $\lambda(\mathbf{x}) = \rho(\mathbf{x})[\alpha(\mathbf{x})^2 - 2\beta(\mathbf{x})^2]$ and $\mu(\mathbf{x}) = \rho(\mathbf{x})\beta(\mathbf{x})^2$, where $\alpha(\mathbf{x})$ and $\beta(\mathbf{x})$ are the P and S wavespeeds. Inhomogeneous terms in (1a,b) represent body sources of seismic waves: $f_i(\mathbf{x},t)$ and $m_{ij}(\mathbf{x},t)$ are components of the force density vector and moment density tensor, respectively. Note that the moment density tensor is split into symmetric and anti-symmetric parts, indicated by superscripts 's' and 'a'.

For FD numerical solution, the wavefield variables in (1a,b) are stored on uniformly-spaced, staggered, spatial and temporal grids. Figure 1 depicts the spatial storage scheme. The primary advantage of staggered storage over alternative non-staggered approaches is greater accuracy in numerical differentiation and interpolation. Enhanced

FD modeling at air-rock interfaces

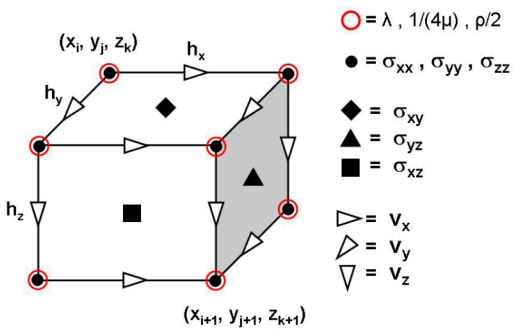

Figure 1. Spatial storage scheme for nine elastodynamic wavefield variables. Three earth model parameters (open red circles) are stored at the corners of the elementary rectangular grid cell.

accuracy leads, in turn, to reduced numerical dispersion in the FD solution of the governing equations. All partial derivatives in (1a,b) are approximated with centered, staggered, FD operators with second-order accuracy in time and N^{th}-order accuracy in space (e.g., Graves, 1996). Explicit time-updating formulae for the nine dependent variables are readily derived.

Earth model parameters λ, μ, and ρ needed for solution of the velocity-stress system are commonly stored on a non-staggered spatial grid (open red circles in figure 1). Temporal updating of the particle velocity vector components requires mass density values interpolated onto velocity storage locations (triangles in figure 1). Let ρ_1 and ρ_2 denote two adjacent stored densities. Then, the interpolated value is given by the arithmetic average

$$\rho_{\text{ave}} = \frac{1}{2}\left(\rho_1 + \rho_2\right).$$

This value is divided into the stress gradient terms in (1a). Similarly, FD updating of shear stress tensor components located on the faces of the elementary grid cell requires interpolated shear moduli. We utilize the harmonic average

$$\frac{1}{\mu_{\text{ave}}} = \frac{1}{4}\left(\frac{1}{\mu_1} + \frac{1}{\mu_2} + \frac{1}{\mu_3} + \frac{1}{\mu_4}\right),$$

where μ_n refer to four surrounding stored values. μ_{ave} could be subsequently multiplied into the velocity gradient terms in equation (1b) (but see below). No spatial averaging of the Lamé parameter λ is necessary for updating the compressional stress tensor components.

The above material parameter averaging approach was developed by Moczo et al. (2002). In numerous tests, we have observed that it yields stable numerical solutions at planar air-rock interfaces, using a standard staggered grid 3D FD algorithm. In contrast, alternative schemes involving arithmetic averaging of mass buoyancy (reciprocal mass density) and shear modulus are unstable.

A reduction in the arithmetic operation count associated with material parameter averaging is achieved by storing $\rho/2$ and $1/4\mu$ at gridpoints. The interpolated shear compliance $c_{ave} = 1/\mu_{ave}$ is then divided into the velocity gradients of (1b). If a shear modulus μ_n at a gridpoint vanishes (in the case where the gridpoint samples an ideal fluid), it is replaced by a very small value during the model storage phase, prior to finite-difference calculations. We have used $\mu = \rho\beta^2$ with β = 0.001 m/s, and have not observed any adverse effects. Alternately, conditional logic can be used to skip the division.

Air-Rock Interface Example

Consider a simple earth model consisting of air (α = 350 ms/, β = 0 m/s, ρ = 1 kg/m^3) overlying competent rock (α = 4000 m/s, β = 2400 m/s, ρ = 2500 kg/m^3). Hence, contrasts in P-wave speed and mass density across the horizontal interface at z = 0 m are 11.4:1 and 2500:1 respectively. A vertical force source is buried 10.5 m below this interface and is activated by a Ricker wavelet with peak frequency 25 Hz (1% amplitude spectrum bandwidth: 2-69 Hz). An array of receivers is distributed vertically across the interface, and is located immediately above the source point (i.e., with *no* horizontal offset).

Despite the close proximity of the seismic energy source to the high-contrast interface, all FD numerical simulations, employing the material parameter averaging approach described above, remain stable. Spatial sampling intervals are $h_x = h_y = h_z$ = 1 m, and the timestep is Δt = 0.120 s, implying that CFL stability parameters for O(2,2) and O(4,4) FD algorithms are less than unity. The fine spatial sampling assures that the shortest wavelength propagating within air is sampled by about five gridpoints. When alternative material parameter averaging schemes are used, these FD simulations go unstable!

Figure 2 illustrates vertical particle velocity (V_z) and pressure (P) traces, calculated with two different spatial differencing schemes in the 3D FD algorithm. For 2nd-order differencing applied to velocities and stresses all waveforms appear reasonable. V_z is continuous across the interface, and is delayed in time as the wave propagates upward into air. It also has the same magnitude within air and rock, consistent with normal incidence reflection and transmission coefficients at the interface (R ≈ −1, T ≈ +2). Pressure (calculated in the FD algorithm as −1/3 times the trace of the stress tensor) is ~10,000 times smaller in air than in rock, also in agreement with theory.

Traces in the right column of figure 2 are calculated with conventional 4th-order spatial differencing of velocity and stress components. In stark contrast to the situation with 2nd-order differencing, large-amplitude oscillatory signals

are observed within air. Although there is closer agreement for the signals recorded within rock, the O(V,S)=O(4,4) waveforms remain inaccurate.

Figure 3 illustrates the analogous set of traces generated by a vertical force source located in air at $z = -10.5$ m, directly above the receiver array. Once again, O(V,S)=O(2,2) calculated waveforms are reasonable, whereas O(4,4) responses in rock are clearly non-physical. Downward- and upward-propagating waves (within air) travel at much lower speed than in figure 2 (within rock), and are thus readily discernable. In this situation, pressure has the same magnitude in both media, and vertical particle velocity is ~10,000 times smaller in rock. Although V_z appears zero near the surface (sampling is ½ grid interval above), it is actually non-zero *on* the surface, consistent with the plane transmission coefficient ($T \approx 7 \times 10^{-5}$).

Spatial Finite-Differencing

Traces displayed in figures 2 and 3 are calculated with time-domain FD algorithms with 2nd-order (two point) and 4th-order (four point) spatial differencing applied to the velocity vector and stress tensor components. Conventional 4th-order differencing produces decidedly inferior results. We surmise the reason for this situation as follows. According to equation (1a), the time rate of change of a velocity component is proportional to a linear combination of spatial derivatives of stress components. At an air-rock interface, the normal components of velocity and stress must be continuous, whereas stress gradients can be discontinuous. When updating a velocity component within air adjacent to the interface, the four-point FD operator "reaches" across the interface and samples stresses within rock. It is physically inappropriate to apply a rock stress (which has far larger magnitude) for updating air particle velocities. A second-order FD operator, with smaller spatial extent, avoids this physical inconsistency by estimating stress gradients only within air.

We have tested this conjecture by calculating seismic responses via a hybrid staggered-grid FD algorithm, where 4th-order spatial differencing is applied to all velocity components, and 2nd-order differencing is applied to all stress components. [We use the symbol O(V,S)=O(4,2) to refer to this situation.] Results identical to the left column of figure 2 are obtained (to within typical visual display scales), thus validating our reasoning. Unfortunately, O(V,S)=O(4,2) differencing does *not* reproduce the favorable results illustrated in the left column of figure 3, where the seismic energy source is situated in air above the interface. In this case, stresses within air and rock are approximately the same, and particle velocities in air exceed those in rock by four orders of magnitude. The converse spatial differencing O(V,S)=O(2,4) yields the desired results in the left column of figure 3, for similar physical/mathematical reasoning. In order for the FD algorithm to accommodate both situations with the desired accuracy, it must utilize symmetric O(V,S)=O(2,2) differencing in the vicinity of high-contrast interfaces. Either asymmetric approach is inadequate.

Obviously, we desire to retain the well-established advantages of 4th-order spatial differencing (i.e., superior numerical phase and group speed performance) throughout the bulk of a 3D earth model where material parameter contrasts are relatively mild. Accordingly, we have implemented a spatial FD operator "switching" scheme, whereby the differencing order is reduced from 4 to 2 at gridpoint locations possessing strong material parameter contrasts with immediate neighbors. Such points are identified prior to FD updating by scanning the 3D earth model grid, and forming dimensionless ratios of parameter values between adjacent gridpoints. The particular threshold value for effecting a "switch" is currently under investigation. Although mass density is clearly the most significant parameter, we have encountered some modeling situations where P- and S-wave speeds also play a role.

There are two approaches for implementing the operator order switching scheme. Currently, we employ conditional logic within the FD updating loops to decide when to change order. No significant slowdown in algorithm execution speed has been observed, although this could depend on overall model size. Alternately, one may segregate the gridpoints into two distinct groups (say, near and remote from high-contrast interfaces), and apply the proper spatial FD operator to each. The latter approach avoids conditional logic, and thus may provide higher algorithm execution speed.

Conclusion and Ongoing Work

Stable and accurate numerical modeling of seismic wave propagation in 3D earth models with large parameter contrasts is obtained via simple modifications to a standard staggered grid O(2,4) FD algorithm. The material parameter averaging scheme advocated by Moczo et al. (2002) achieves stability. Reduction of the spatial differencing order from 4 to 2 in the immediate vicinity of high-contrast interfaces yields superior accuracy.

Current efforts involve implementing the spatial order switching scheme in a computationally efficient manner, as well as quantitatively understanding the critical threshold value(s) mandating a change in order. Finally, we are examining the accuracy of the various spatial differencing approaches for simulating coupled air-rock interface waves, along plane or non-plane material discontinuity surfaces.

Acknowledgment

Sandia National Laboratories is a multiprogram science and engineering facility operated by Sandia Corporation, a Lockheed-Martin company, for the US Department of Energy's National Nuclear Security Administration, under contract DE-AC04-94AL850.

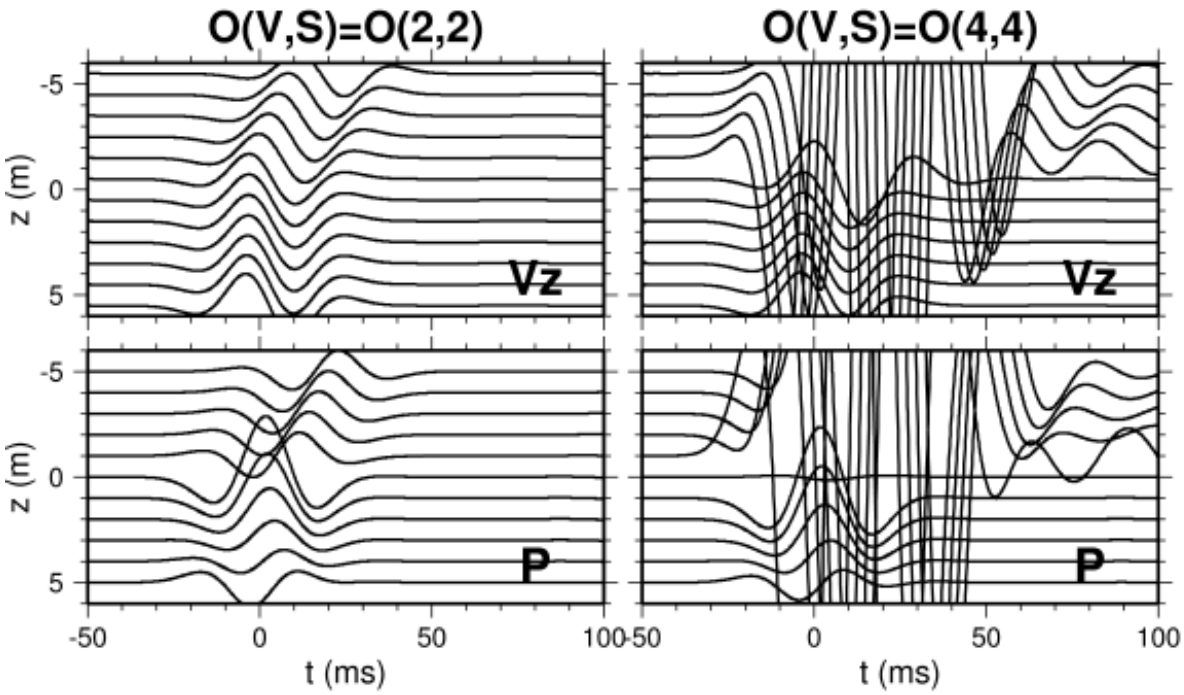

Figure 2. Vertical particle velocity (Vz) and pressure (P) traces generated by a vertical force (Fz) source located in **rock** at z = +10.5 m. Left and right columns correspond to 2nd-order and 4th-order spatial differencing applied to velocity and stress components. All velocity traces are displayed with identical gain, whereas pressure traces recorded in air ($z < 0$) are amplified by 10,000 compared to pressure traces recorded in rock ($z \geq 0$).

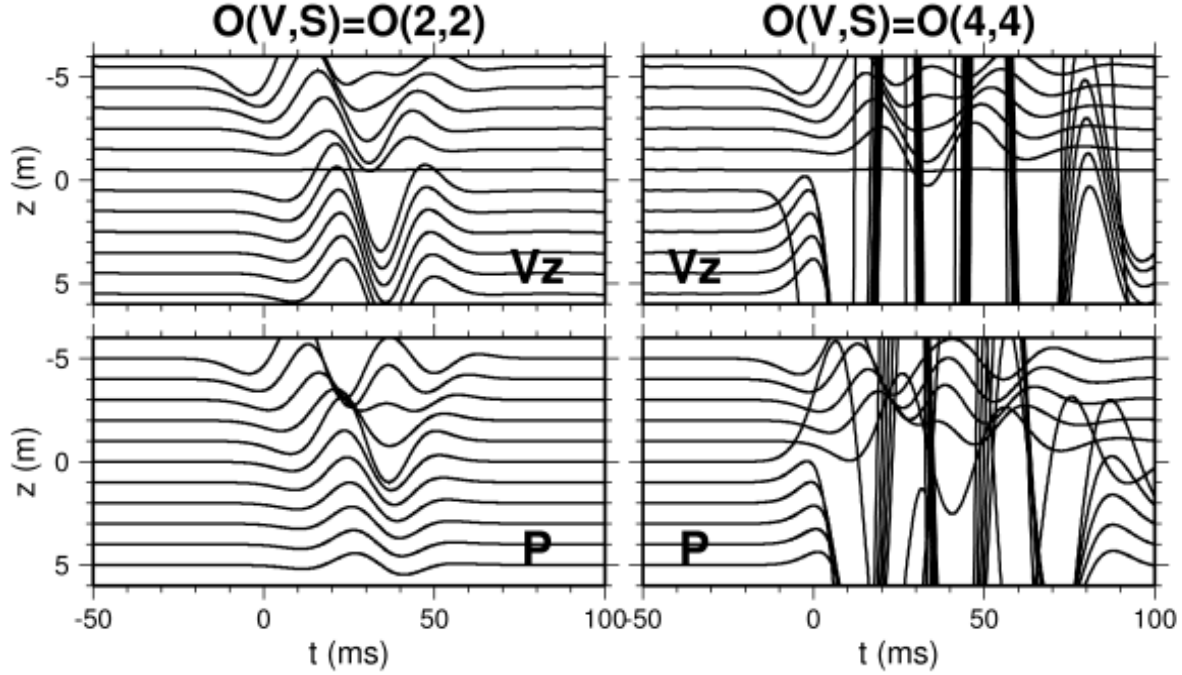

Figure 3. Analogous traces generated by a vertical force source located in **air** at z = –10.5 m. All pressure traces are displayed with the same gain, whereas velocity traces recorded in rock are amplified by 10,000 compared to velocity traces recorded in air.

References

Bartel, L.C., N.P. Symons, N.P., and D.F. Aldridge, 2000, Graded boundary simulation of air/earth interfaces in finite-difference elastic wave modeling: 70th Annual International Meeting, Soc. Expl. Geophys., Expanded Abstracts, 2444-2447.

Cunha, C.A., 1993, Elastic modeling in discontinuous media: Geophysics, **59**, 1840-1851.

Frankel, A., and W. Leith, 1992, Evaluation of effects on the P and S-waves of explosions at the northern Novaya Zemlya test site using 3-D numerical simulations: Geophysical Research Letters, **19**, 1887-1980.

Graves, R.W., 1996, Simulating seismic wave propagation in 3D elastic media using staggered-grid finite differences: Bulletin of the Seismological Society of America, **86**, 1091-1106.

Haney, M.M., 2007, Generalization of von Neumann analysis for a model of two discrete half-spaces: The acoustic case: Geophysics, **72**, SM35-SM46.

Moczo, P., J. Kristek, V. Vavrycuk, R.J. Archuleta, and L. Halada., 2002, 3D heterogeneous staggered-grid finite-difference modeling of seismic motion with volume harmonic and arithmetic averaging of elastic moduli and densities: Bulletin of the Seismological Society of America, **92**, 3042-3066.

Muir, F., J. Dellinger, J. Etgen, and D. Nichols, 1992, Modeling elastic fields across irregular boundaries: Geophysics, **57**, 1189-1193.

Schultz, C.A., 1997, A density-tapering approach for modeling the seismic response of free-surface topography: Geophysical Research Letters, **24**, 2809-2812.

Saenger, E.H., N. Gold, and S.A. Shapiro, 2004, Modeling the propagation of elastic waves using a modified finite-difference grid: Wave Motion, **31**, 77-92.

Zahradnik, J., P. Moczo, and F. Hron, 1993, Testing four elastic finite-difference schemes for behavior at discontinuities: Bulletin of the Seismological Society of America, **83**, 107-129.